

Observation of the electromagnetic doubly OZI-suppressed decay $J/\psi \rightarrow \phi\pi^0$

M. Ablikim¹, M. N. Achasov^{9,a}, X. C. Ai¹, O. Albayrak⁵, M. Albrecht⁴, D. J. Ambrose⁴⁴, A. Amoroso^{48A,48C}, F. F. An¹, Q. An⁴⁵, J. Z. Bai¹, R. Baldini Ferroli^{20A}, Y. Ban³¹, D. W. Bennett¹⁹, J. V. Bennett⁵, M. Bertani^{20A}, D. Bettoni^{21A}, J. M. Bian⁴³, F. Bianchi^{48A,48C}, E. Boger^{23,h}, O. Bondarenko²⁵, I. Boyko²³, R. A. Briere⁵, H. Cai⁵⁰, X. Cai¹, O. Cakir^{40A,b}, A. Calcaterra^{20A}, G. F. Cao¹, S. A. Cetin^{40B}, J. F. Chang¹, G. Chelkov^{23,c}, G. Chen¹, H. S. Chen¹, H. Y. Chen², J. C. Chen¹, M. L. Chen¹, S. J. Chen²⁹, X. Chen¹, X. R. Chen²⁶, Y. B. Chen¹, H. P. Cheng¹⁷, X. K. Chu³¹, G. Cibinetto^{21A}, D. Cronin-Hennessy⁴³, H. L. Dai¹, J. P. Dai³⁴, A. Dbeyssi¹⁴, D. Dedovich²³, Z. Y. Deng¹, A. Denig²², I. Denysenko²³, M. Destefanis^{48A,48C}, F. De Mori^{48A,48C}, Y. Ding²⁷, C. Dong³⁰, J. Dong¹, L. Y. Dong¹, M. Y. Dong¹, S. X. Du⁵², P. F. Duan¹, J. Z. Fan³⁹, J. Fang¹, S. S. Fang¹, X. Fang⁴⁵, Y. Fang¹, L. Fava^{48B,48C}, F. Feldbauer²², G. Felici^{20A}, C. Q. Feng⁴⁵, E. Fioravanti^{21A}, M. Fritsch^{14,22}, C. D. Fu¹, Q. Gao¹, X. Y. Gao², Y. Gao³⁹, Z. Gao⁴⁵, I. Garzia^{21A}, C. Geng⁴⁵, K. Goetzen¹⁰, W. X. Gong¹, W. Gradl²², M. Greco^{48A,48C}, M. H. Gu¹, Y. T. Gu¹², Y. H. Guan¹, A. Q. Guo¹, L. B. Guo²⁸, Y. Guo¹, Y. P. Guo²², Z. Haddadi²⁵, A. Hafner²², S. Han⁵⁰, Y. L. Han¹, X. Q. Hao¹⁵, F. A. Harris⁴², K. L. He¹, Z. Y. He³⁰, T. Held⁴, Y. K. Heng¹, Z. L. Hou¹, C. Hu²⁸, H. M. Hu¹, J. F. Hu^{48A,48C}, T. Hu¹, Y. Hu¹, G. M. Huang⁶, G. S. Huang⁴⁵, H. P. Huang⁵⁰, J. S. Huang¹⁵, X. T. Huang³³, Y. Huang²⁹, T. Hussain⁴⁷, Q. Ji¹, Q. P. Ji³⁰, X. B. Ji¹, X. L. Ji¹, L. L. Jiang¹, L. W. Jiang⁵⁰, X. S. Jiang¹, J. B. Jiao³³, Z. Jiao¹⁷, D. P. Jin¹, S. Jin¹, T. Johansson⁴⁹, A. Julin⁴³, N. Kalantar-Nayestanaki²⁵, X. L. Kang¹, X. S. Kang³⁰, M. Kavatsyuk²⁵, B. C. Ke⁵, R. Kliemt¹⁴, B. Kloss²², O. B. Kolcu^{40B,d}, B. Kopf⁴, M. Kornicer⁴², W. Kühn²⁴, A. Kupsc⁴⁹, W. Lai¹, J. S. Lange²⁴, M. Lara¹⁹, P. Larin¹⁴, C. Leng^{48C}, C. H. Li¹, Cheng Li⁴⁵, D. M. Li⁵², F. Li¹, G. Li¹, H. B. Li¹, J. C. Li¹, Jin Li³², K. Li¹³, K. Li³³, Lei Li³, P. R. Li⁴¹, T. Li³³, W. D. Li¹, W. G. Li¹, X. L. Li³³, X. M. Li¹², X. N. Li¹, X. Q. Li³⁰, Z. B. Li³⁸, H. Liang⁴⁵, Y. F. Liang³⁶, Y. T. Liang²⁴, G. R. Liao¹¹, D. X. Lin¹⁴, B. J. Liu¹, C. X. Liu¹, F. H. Liu³⁵, Fang Liu¹, Feng Liu⁶, H. B. Liu¹², H. H. Liu¹, H. H. Liu¹⁶, H. M. Liu¹, J. Liu¹, J. P. Liu⁵⁰, J. Y. Liu¹, K. Liu³⁹, K. Y. Liu²⁷, L. D. Liu³¹, P. L. Liu¹, Q. Liu⁴¹, S. B. Liu⁴⁵, X. L. Liu²⁶, X. X. Liu⁴¹, Y. B. Liu³⁰, Z. A. Liu¹, Zhiqiang Liu¹, Zhiqing Liu²², H. Loehner²⁵, X. C. Lou^{1,e}, H. J. Lu¹⁷, J. G. Lu¹, R. Q. Lu¹⁸, Y. Lu¹, Y. P. Lu¹, C. L. Luo²⁸, M. X. Luo⁵¹, T. Luo⁴², X. L. Luo¹, M. Lv¹, X. R. Lyu⁴¹, F. C. Ma²⁷, H. L. Ma¹, L. L. Ma³³, Q. M. Ma¹, S. Ma¹, T. Ma¹, X. N. Ma³⁰, X. Y. Ma¹, F. E. Maas¹⁴, M. Maggiora^{48A,48C}, Q. A. Malik⁴⁷, Y. J. Mao³¹, Z. P. Mao¹, S. Marcello^{48A,48C}, J. G. Messchendorp²⁵, J. Min¹, T. J. Min¹, R. E. Mitchell¹⁹, X. H. Mo¹, Y. J. Mo⁶, C. Morales Morales¹⁴, K. Moriya¹⁹, N. Yu. Muchnoi^{9,a}, H. Muramatsu⁴³, Y. Nefedov²³, F. Nerling¹⁴, I. B. Nikolaev^{9,a}, Z. Ning¹, S. Nisar⁸, S. L. Niu¹, X. Y. Niu¹, S. L. Olsen³², Q. Ouyang¹, S. Pacetti^{20B}, P. Patteri^{20A}, M. Pelizaeus⁴, H. P. Peng⁴⁵, K. Peters¹⁰, J. Pettersson⁴⁹, J. L. Ping²⁸, R. G. Ping¹, R. Poling⁴³, Y. N. Pu¹⁸, M. Qi²⁹, S. Qian¹, C. F. Qiao⁴¹, L. Q. Qin³³, N. Qin⁵⁰, X. S. Qin¹, Y. Qin³¹, Z. H. Qin¹, J. F. Qiu¹, K. H. Rashid⁴⁷, C. F. Redmer²², H. L. Ren¹⁸, M. Ripka²², G. Rong¹, X. D. Ruan¹², V. Santoro^{21A}, A. Sarantsev^{23,f}, M. Savrié^{21B}, K. Schoenning⁴⁹, S. Schumann²², W. Shan³¹, M. Shao⁴⁵, C. P. Shen², P. X. Shen³⁰, X. Y. Shen¹, H. Y. Sheng¹, W. M. Song¹, X. Y. Song¹, S. Sosio^{48A,48C}, S. Spataro^{48A,48C}, G. X. Sun¹, J. F. Sun¹⁵, S. S. Sun¹, Y. J. Sun⁴⁵, Y. Z. Sun¹, Z. J. Sun¹, Z. T. Sun¹⁹, C. J. Tang³⁶, X. Tang¹, I. Tapan^{40C}, E. H. Thorndike⁴⁴, M. Tiemens²⁵, D. Toth⁴³, M. Ullrich²⁴, I. Uman^{40B}, G. S. Varner⁴², B. Wang³⁰, B. L. Wang⁴¹, D. Wang³¹, D. Y. Wang³¹, K. Wang¹, L. L. Wang¹, L. S. Wang³³, M. Wang³³, P. Wang¹, P. L. Wang¹, Q. J. Wang¹, S. G. Wang³¹, W. Wang¹, X. F. Wang³⁹, Y. D. Wang^{20A}, Y. F. Wang¹, Y. Q. Wang²², Z. Wang¹, Z. G. Wang¹, Z. H. Wang⁴⁵, Z. Y. Wang¹, T. Weber²², D. H. Wei¹¹, J. B. Wei³¹, P. Weidenkaff²², S. P. Wen¹, U. Wiedner⁴, M. Wolke⁴⁹, L. H. Wu¹, Z. Wu¹, L. G. Xia³⁹, Y. Xia¹⁸, D. Xiao¹, Z. J. Xiao²⁸, Y. G. Xie¹, Q. L. Xiu¹, G. F. Xu¹, L. Xu¹, Q. J. Xu¹³, Q. N. Xu⁴¹, X. P. Xu³⁷, L. Yan⁴⁵, W. B. Yan⁴⁵, W. C. Yan⁴⁵, Y. H. Yan¹⁸, H. X. Yang¹, L. Yang⁵⁰, Y. Yang⁶, Y. X. Yang¹¹, H. Ye¹, M. Ye¹, M. H. Ye⁷, J. H. Yin¹, B. X. Yu¹, C. X. Yu³⁰, H. W. Yu³¹, J. S. Yu²⁶, C. Z. Yuan¹, W. L. Yuan²⁹, Y. Yuan¹, A. Yuncu^{40B,g}, A. A. Zafar⁴⁷, A. Zallo^{20A}, Y. Zeng¹⁸, B. X. Zhang¹, B. Y. Zhang¹, C. Zhang²⁹, C. C. Zhang¹, D. H. Zhang¹, H. H. Zhang³⁸, H. Y. Zhang¹, J. J. Zhang¹, J. L. Zhang¹, J. Q. Zhang¹, J. W. Zhang¹, J. Y. Zhang¹, J. Z. Zhang¹, K. Zhang¹, L. Zhang¹, S. H. Zhang³³, X. Y. Zhang³³, Y. Zhang¹, Y. H. Zhang¹, Y. T. Zhang⁴⁵, Z. H. Zhang⁶, Z. P. Zhang⁴⁵, Z. Y. Zhang⁵⁰, G. Zhao¹, J. W. Zhao¹, J. Y. Zhao¹, J. Z. Zhao¹, Lei Zhao⁴⁵, Ling Zhao¹, M. G. Zhao³⁰, Q. Zhao¹, Q. W. Zhao¹, S. J. Zhao⁵², T. C. Zhao¹, Y. B. Zhao¹, Z. G. Zhao⁴⁵, A. Zhemchugov^{23,h}, B. Zheng⁴⁶, J. P. Zheng¹, W. J. Zheng³³, Y. H. Zheng⁴¹, B. Zhong²⁸, L. Zhou¹, Li Zhou³⁰, X. Zhou⁵⁰, X. K. Zhou⁴⁵, X. R. Zhou⁴⁵, X. Y. Zhou¹, K. Zhu¹, K. J. Zhu¹, S. Zhu¹, X. L. Zhu³⁹, Y. C. Zhu⁴⁵, Y. S. Zhu¹, Z. A. Zhu¹, J. Zhuang¹, L. Zotti^{48A,48C}, B. S. Zou¹, J. H. Zou¹

(BESIII Collaboration)

¹ Institute of High Energy Physics, Beijing 100049, People's Republic of China² Beihang University, Beijing 100191, People's Republic of China³ Beijing Institute of Petrochemical Technology, Beijing 102617, People's Republic of China⁴ Bochum Ruhr-University, D-44780 Bochum, Germany⁵ Carnegie Mellon University, Pittsburgh, Pennsylvania 15213, USA⁶ Central China Normal University, Wuhan 430079, People's Republic of China

- ⁷ China Center of Advanced Science and Technology, Beijing 100190, People's Republic of China
- ⁸ COMSATS Institute of Information Technology, Lahore, Defence Road, Off Raiwind Road, 54000 Lahore, Pakistan
- ⁹ G.I. Budker Institute of Nuclear Physics SB RAS (BINP), Novosibirsk 630090, Russia
- ¹⁰ GSI Helmholtzcentre for Heavy Ion Research GmbH, D-64291 Darmstadt, Germany
- ¹¹ Guangxi Normal University, Guilin 541004, People's Republic of China
- ¹² GuangXi University, Nanning 530004, People's Republic of China
- ¹³ Hangzhou Normal University, Hangzhou 310036, People's Republic of China
- ¹⁴ Helmholtz Institute Mainz, Johann-Joachim-Becher-Weg 45, D-55099 Mainz, Germany
- ¹⁵ Henan Normal University, Xinxiang 453007, People's Republic of China
- ¹⁶ Henan University of Science and Technology, Luoyang 471003, People's Republic of China
- ¹⁷ Huangshan College, Huangshan 245000, People's Republic of China
- ¹⁸ Hunan University, Changsha 410082, People's Republic of China
- ¹⁹ Indiana University, Bloomington, Indiana 47405, USA
- ²⁰ (A)INFN Laboratori Nazionali di Frascati, I-00044, Frascati, Italy; (B)INFN and University of Perugia, I-06100, Perugia, Italy
- ²¹ (A)INFN Sezione di Ferrara, I-44122, Ferrara, Italy; (B)University of Ferrara, I-44122, Ferrara, Italy
- ²² Johannes Gutenberg University of Mainz, Johann-Joachim-Becher-Weg 45, D-55099 Mainz, Germany
- ²³ Joint Institute for Nuclear Research, 141980 Dubna, Moscow region, Russia
- ²⁴ Justus Liebig University Giessen, II. Physikalisches Institut, Heinrich-Buff-Ring 16, D-35392 Giessen, Germany
- ²⁵ KVI-CART, University of Groningen, NL-9747 AA Groningen, The Netherlands
- ²⁶ Lanzhou University, Lanzhou 730000, People's Republic of China
- ²⁷ Liaoning University, Shenyang 110036, People's Republic of China
- ²⁸ Nanjing Normal University, Nanjing 210023, People's Republic of China
- ²⁹ Nanjing University, Nanjing 210093, People's Republic of China
- ³⁰ Nankai University, Tianjin 300071, People's Republic of China
- ³¹ Peking University, Beijing 100871, People's Republic of China
- ³² Seoul National University, Seoul, 151-747 Korea
- ³³ Shandong University, Jinan 250100, People's Republic of China
- ³⁴ Shanghai Jiao Tong University, Shanghai 200240, People's Republic of China
- ³⁵ Shanxi University, Taiyuan 030006, People's Republic of China
- ³⁶ Sichuan University, Chengdu 610064, People's Republic of China
- ³⁷ Soochow University, Suzhou 215006, People's Republic of China
- ³⁸ Sun Yat-Sen University, Guangzhou 510275, People's Republic of China
- ³⁹ Tsinghua University, Beijing 100084, People's Republic of China
- ⁴⁰ (A)Istanbul Aydin University, 34295 Sefakoy, Istanbul, Turkey; (B)Dogus University, 34722 Istanbul, Turkey; (C)Uludag University, 16059 Bursa, Turkey
- ⁴¹ University of Chinese Academy of Sciences, Beijing 100049, People's Republic of China
- ⁴² University of Hawaii, Honolulu, Hawaii 96822, USA
- ⁴³ University of Minnesota, Minneapolis, Minnesota 55455, USA
- ⁴⁴ University of Rochester, Rochester, New York 14627, USA
- ⁴⁵ University of Science and Technology of China, Hefei 230026, People's Republic of China
- ⁴⁶ University of South China, Hengyang 421001, People's Republic of China
- ⁴⁷ University of the Punjab, Lahore-54590, Pakistan
- ⁴⁸ (A)University of Turin, I-10125, Turin, Italy; (B)University of Eastern Piedmont, I-15121, Alessandria, Italy; (C)INFN, I-10125, Turin, Italy
- ⁴⁹ Uppsala University, Box 516, SE-75120 Uppsala, Sweden
- ⁵⁰ Wuhan University, Wuhan 430072, People's Republic of China
- ⁵¹ Zhejiang University, Hangzhou 310027, People's Republic of China
- ⁵² Zhengzhou University, Zhengzhou 450001, People's Republic of China
- ^a Also at the Novosibirsk State University, Novosibirsk, 630090, Russia
- ^b Also at Ankara University, 06100 Tandogan, Ankara, Turkey
- ^c Also at the Moscow Institute of Physics and Technology, Moscow 141700, Russia and at the Functional Electronics Laboratory, Tomsk State University, Tomsk, 634050, Russia
- ^d Currently at Istanbul Arel University, 34295 Istanbul, Turkey
- ^e Also at University of Texas at Dallas, Richardson, Texas 75083, USA
- ^f Also at the NRC "Kurchatov Institute", PNPI, 188300, Gatchina, Russia
- ^g Also at Bogazici University, 34342 Istanbul, Turkey
- ^h Also at the Moscow Institute of Physics and Technology, Moscow 141700, Russia

Using a sample of 1.31 billion J/ψ events accumulated with the BESIII detector at the BEPCII collider, we report the observation of the decay $J/\psi \rightarrow \phi\pi^0$, which is the first evidence for a doubly Okubo-Zweig-Iizuka suppressed electromagnetic J/ψ decay. A clear structure is observed in the K^+K^- mass spectrum around $1.02 \text{ GeV}/c^2$, which can be attributed to interference between $J/\psi \rightarrow \phi\pi^0$ and $J/\psi \rightarrow K^+K^-\pi^0$ decays. Due to this interference, two possible solutions are found. The corresponding measured values of the branching fraction of $J/\psi \rightarrow \phi\pi^0$ are $[2.94 \pm 0.16(\text{stat.}) \pm 0.16(\text{syst.})] \times 10^{-6}$ and $[1.24 \pm 0.33(\text{stat.}) \pm 0.30(\text{syst.})] \times 10^{-7}$.

PACS numbers: 13.25.Gv, 14.40.Be

The discovery of the J/ψ played an important role in understanding the basic constituents of nature and opened a new era in particle physics. Its unexpected narrow decay width provided insight into the study of strong interactions. As its mass is below the charmed meson pair threshold, direct decay into charmed mesons is forbidden. Therefore the J/ψ hadronic decay modes are Okubo-Zweig-Iizuka (OZI) [1] suppressed, and the final states are composed only of light hadrons.

A full investigation of J/ψ decaying to a vector meson (V) and a pseudoscalar meson (P) can provide rich information about SU(3) flavor symmetry and its breaking, probe the quark and gluon content of the pseudoscalar mesons, and determine the electromagnetic amplitudes [2–4]. However the presence of doubly OZI (DOZI) suppressed processes, like the observation of J/ψ radiatively decaying into $\omega\phi$ [5, 6], complicates matters as they do not obey quark correlation or satisfy nonet symmetry (treating SU(3) octets and singlet as a nonet and assuming the coupling constants are the same in the interactions [2, 3]). Well established phenomenological models [2, 3] have indicated that the DOZI amplitude can have a large impact through interference with the singly OZI suppressed amplitude.

Of interest is the decay $J/\psi \rightarrow \phi\pi^0$, which occurs via the electromagnetic DOZI process or by non-ideal $\omega - \phi$ mixing [2, 3, 7]. Recently, using a combination of a factorization scheme for the strong decays and a Vector Meson Dominance (VMD) model for electromagnetic decays in $J/\psi \rightarrow VP$, the branching fraction of $J/\psi \rightarrow \phi\pi^0$ has been predicted to be around 8×10^{-7} [8], while the best upper limit to date comes from the BES collaboration, $\mathcal{B}(J/\psi \rightarrow \phi\pi^0) < 6.4 \times 10^{-6}$ at the 90% confidence level (C.L.) [9]. In this paper, we report the first observation of $J/\psi \rightarrow \phi\pi^0$ based on a sample of $(1.311 \pm 0.011) \times 10^9$ J/ψ events [10, 11] accumulated with the BESIII detector.

The BESIII detector [12] is a magnetic spectrometer located at the Beijing Electron Positron Col-

lider (BEPCII), which is a double-ring e^+e^- collider with a design peak luminosity of $10^{33} \text{ cm}^{-2}\text{s}^{-1}$ at the center of mass (c.m.) energy of 3.773 GeV. The cylindrical core of the BESIII detector consists of a helium-based main drift chamber (MDC), a plastic scintillator time-of-flight system (TOF), and a CsI(Tl) electromagnetic calorimeter (EMC). All of them are enclosed in a superconducting solenoidal magnet providing a 1.0 T (0.9 T in 2012) magnetic field. The solenoid is supported by an octagonal flux-return yoke with resistive plate counter muon identifier modules interleaved with steel. The acceptance for charged particles and photons is 93% of 4π solid angle. The charged-particle momentum resolution is 0.5% at 1 GeV/c, and the specific energy loss (dE/dx) resolution is 6%. The EMC measures photon energies with a resolution of 2.5% (5%) at 1 GeV in the barrel (endcaps). The time resolution of the TOF is 80 ps in the barrel and 110 ps in the endcaps. The BESIII offline software system (BOSS) framework is based on Gaudi [13]. A GEANT4-based [14] Monte Carlo (MC) simulation is used to determine detection efficiencies and estimate backgrounds.

For the decay $J/\psi \rightarrow \phi\pi^0 \rightarrow K^+K^-\gamma\gamma$, a candidate event is required to have two charged tracks with opposite charge and at least two photons. For each charged track, the polar angle in the MDC must satisfy $|\cos\theta| < 0.93$, and the point of closest approach to the e^+e^- interaction point must be within ± 10 cm in the beam direction and within 1 cm in the plane perpendicular to the beam direction. TOF and dE/dx information are combined to give particle identification (PID) probabilities for π , K and p hypotheses. To identify a track as a kaon, the PID probability for the kaon hypothesis must be larger than that for the pion hypothesis.

For each photon, the energy deposited in the EMC must be at least 25 MeV for $|\cos\theta| < 0.8$ or 50 MeV for $0.86 < |\cos\theta| < 0.92$. To select isolated showers, the angle relative to the nearest charged track must be larger than 20° . The timing information of the EMC is used to suppress electronic noise and

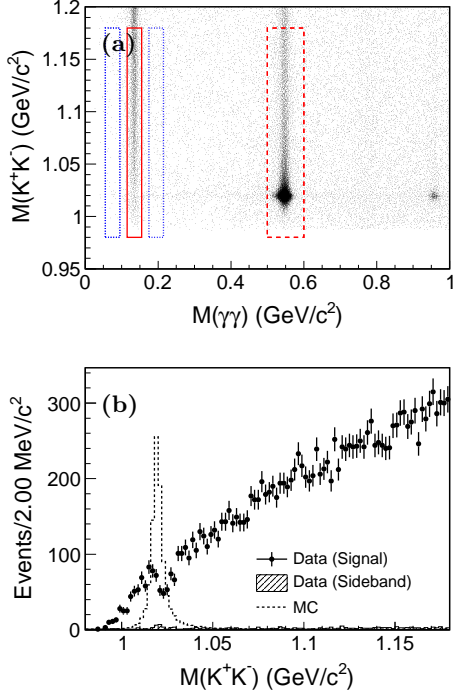


FIG. 1. (a) Scatter plot of $M(K^+K^-)$ versus $M(\gamma\gamma)$. The red solid and blue dotted boxes are the π^0 signal and sideband regions. The red dashed box indicates $J/\psi \rightarrow \phi\eta$. (b) K^+K^- mass spectrum, where the dots with error bars are events in the π^0 signal region; the hatched histogram are events from the π^0 sidebands; and the dashed histogram is MC simulation of $J/\psi \rightarrow \phi\pi^0$ with arbitrary normalization.

unrelated energy deposits. Furthermore, a four-constraint (4C) kinematic fit is applied to the candidate events under the $K^+K^-\gamma\gamma$ hypothesis, requiring the 4-momentum of the final state to be equal to that of the colliding beams. If there are more than two photon candidates in an event, the combination with the smallest $\chi_{4C}^2(K^+K^-\gamma\gamma)$ is retained. Events with $\chi_{4C}^2 < 30$ are selected.

After the above selection, the scatter plot of $M(K^+K^-)$ versus $M(\gamma\gamma)$ (Fig. 1 (a)) shows two clear clusters corresponding to $\phi\eta$ and $\phi\eta'$ and two bands corresponding to $K^+K^-\pi^0$ and $K^+K^-\eta$, but no evident accumulation of events for $\phi\pi^0$. To investigate the $M(K^+K^-)$ spectrum of $K^+K^-\pi^0$ events, we select events where the $\gamma\gamma$ invariant mass is in the π^0 mass region $0.115 < M(\gamma\gamma) < 0.155$ GeV/c^2 . The $M(K^+K^-)$ distribution for these events is shown in Fig. 1 (b), where a clear structure around the ϕ mass is seen.

Studies were performed using both MC events and data to investigate whether the structure around

TABLE I. Background analysis for the decay $J/\psi \rightarrow \phi\pi^0$.

Type	Reactions
Coherent	$J/\psi \rightarrow K^+K^-\pi^0$
ϕ peaking	$e^+e^- \rightarrow \gamma_{ISR}\phi, J/\psi \rightarrow \phi\pi^0\pi^0/\phi\gamma\gamma$
π^0 peaking	$J/\psi \rightarrow \gamma\eta_c(1S) \rightarrow \gamma K^+K^-\pi^0$
Other	$J/\psi \rightarrow \gamma K^+K^-/\gamma\pi^0 K^+K^-/\pi^0\pi^0 K^+K^-$

1.02 GeV/c^2 could be background related. We analyze a MC sample of 1.2×10^9 J/ψ inclusive decays, in which the known decay modes were generated by BesEvtGen [15, 16] with measured branching fractions [17] while unknown decays were generated by Lund-Charm [18]. The dominant background events are found to be from $J/\psi \rightarrow K^+K^-\pi^0$ with the intermediate states decaying into $K^\pm\pi^0$ and K^+K^- , which is coherent for the decay $J/\psi \rightarrow \phi\pi^0$. A partial wave analysis, not including $J/\psi \rightarrow \phi\pi^0$ but considering the interference of all intermediate states, yields a smooth distribution with K^+K^- mass below 1.2 GeV/c^2 . The incoherent background can be categorized into three classes as follows. (1) The ϕ peaking background: $e^+e^- \rightarrow \gamma_{ISR}\phi$ and $J/\psi \rightarrow \phi\pi^0\pi^0/\phi\gamma\gamma$. The former background is studied using data taken at energies far from any charmonium resonance and the latter ones are studied by exclusive MC samples. The studies show that these background events can be compensated by the π^0 mass sideband events, which are defined as $0.055 < M(\gamma\gamma) < 0.095$ GeV/c^2 and $0.175 < M(\gamma\gamma) < 0.215$ GeV/c^2 . (2) The π^0 peaking background: $J/\psi \rightarrow \gamma\eta_c(1S) \rightarrow \gamma K^+K^-\pi^0$. This background cannot be taken into account by the π^0 mass sideband events. From MC simulations, the ratio between the number of this background events and the number of the coherent background events in the π^0 mass region is 0.5%. As little is known about the possible intermediate states, we neglect this background and consider the related systematic uncertainty. (3) The non- ϕ and non- π^0 background are dominated by the decays $J/\psi \rightarrow \gamma K^+K^-$, $\gamma\pi^0 K^+K^-$ and $\pi^0\pi^0 K^+K^-$ with various intermediate states. MC simulations show they can be subtracted by the π^0 mass sideband events. All background types are summarized in Table I. Through the studies above, none of these background events produce a structure in the K^+K^- mass spectrum. In addition, the detection efficiency as a function of $M(K^+K^-)$, obtained from the MC simulation and taking into account the angular distributions [19], is also smooth over the K^+K^- mass region, with no structure in the region of the ϕ signal.

A possible explanation for the structure in the $M(K^+K^-)$ spectrum is interference between $J/\psi \rightarrow \phi\pi^0$ and other processes with the same final state. We have verified this using a statistical hypothesis test [20, 21]. In the null hypothesis without $J/\psi \rightarrow \phi\pi^0$, a second-order polynomial function, defined as $F_{H_0} = P(m) \equiv c_0 + c_1m + c_2m^2$, is used in the fit to describe the data after subtraction of the π^0 -sideband events. The positive hypothesis is characterized by a two-component function (F_{H_1}), in which the model is a coherent sum of a relativistic Breit-Wigner resonance and the second-order polynomial function, convoluted with a Gaussian function $G(m, \sigma_m)$ to take into account the mass resolution, σ_m .

$$F_{H_1} = |\sqrt{P(m)/\Phi(m)} + A_\phi(m)|^2 \Phi(m) \otimes G(m, \sigma_m), \quad (1)$$

where

$$A_\phi(m) = \frac{\sqrt{R}e^{i\delta} p_\phi(m) p_K(m) B(p_\phi(m)) B(p_K(m))}{m^2 - m_\phi^2 + im\Gamma(m) B(p_\phi(m_0)) B(p_K(m_0))}, \quad (2)$$

with

$$\Gamma(m) \equiv \left(\frac{p_K(m)}{p_K(m_0)} \right)^3 \frac{m_0 B(p_K(m))}{m B(p_K(m_0))} \Gamma_0. \quad (3)$$

Here, m is the K^+K^- invariant mass. m_0 and Γ_0 are the nominal mass and decay width of the ϕ [17]. $p_\phi(m)$ ($p_K(m)$) is the momentum of the ϕ (K) in the frame of J/ψ (ϕ) with the mass of ϕ being m . $\Phi(m) = p_\phi(m)p_K(m)$ is the phase space factor. $B(p)$, defined as $B(p) \equiv 1/\sqrt{1 + (rp)^2}$, is the Blatt-Weisskopf penetration form factor [22] with the meson radius r being 3 GeV^{-1} . R and δ represents the magnitude and relative phase angle respectively for the contribution of the ϕ resonance. Omitting the convolution, F_{H_1} can be expanded to be

$$P(m) + |A_\phi(m)|^2 \Phi(m) + 2\sqrt{P(m)\Phi(m)} \Re A_\phi(m), \quad (4)$$

where the first term is the non- ϕ contribution from the decay $J/\psi \rightarrow K^+K^-\pi^0$; the second term is the ϕ resonance from the decay $J/\psi \rightarrow \phi\pi^0$; and the third term is their interference. Here, $\Re A_\phi(m)$ denotes the real part of $A_\phi(m)$.

MC simulations show that the K^+K^- mass resolutions are essentially the same for J/ψ decaying to $\phi\pi^0$ and $\phi\eta$ with $\pi^0/\eta \rightarrow \gamma\gamma$. We obtain $\sigma_m = (1.00 \pm 0.02) \text{ MeV}/c^2$ by performing an unbinned likelihood fit to the $M(K^+K^-)$ spectrum of $J/\psi \rightarrow \phi\eta$ with $0.50 < M(\gamma\gamma) < 0.60 \text{ GeV}/c^2$, shown in the red dashed box in Fig. 1 (a). The

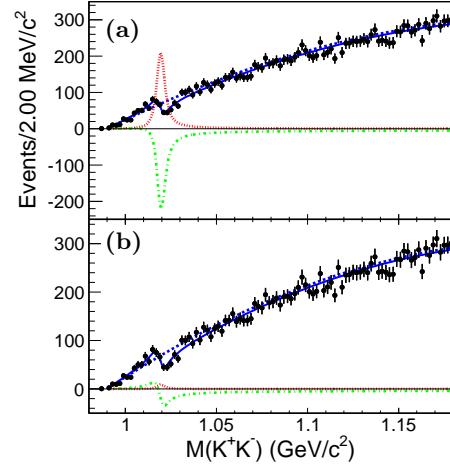


FIG. 2. Fit to $M(K^+K^-)$ spectrum after sideband subtraction for Solution I (a) and Solution II (b). The red dotted curve denotes the ϕ resonance; the blue dashed curve is the non- ϕ contribution; the green dot-dashed curve represents their interference; and the blue solid curve is the sum of them.

same Breit-Wigner formula convoluted with a Gaussian function is used to describe the ϕ signal, while a second-order polynomial is used to describe the background.

After subtracting the incoherent background events estimated with π^0 sidebands, a maximum likelihood fit is performed to the $M(K^+K^-)$ distribution under the positive hypothesis. Two solutions with two different phase angles between the ϕ resonance and the non- ϕ contributions are found. The final fits, including the individual contributions of each component, are illustrated in Fig. 2 (a) and Fig. 2 (b), while the signal yields and the relative phase angles are summarized in Table II. In Fig. 2 (a) and Fig. 2 (b), the blue dashed curve is the non- ϕ contribution (the first term in Eq. 4); the red dotted curve denotes the ϕ resonance (the second term in Eq. 4); the green dot-dashed curve represents their interference (the third term in Eq. 4); and the blue solid curve is the sum of them. The signal yield N^{sig} in Table II is calculated by integrating the function of the ϕ resonance over the fit range. The statistical significance is determined by the change of the log likelihood value and the number of degrees of freedom in the fit with and without the ϕ signal [20, 23]. Both solutions have a statistical significance of 6.4σ , which means that they provide identically good descriptions of data.

The non-resonant quantum electrodynamics (QED) contribution is estimated in two ways. One way is by analyzing data taken at energies far from

TABLE II. Fit results. N^{sig} is the fitted number of signal events (from the parameter R). δ is the relative phase. $2\Delta \log \mathcal{L}$ is 2 times the difference of the log-likelihood value with and without ϕ signal, while N_f is the change of the number of degrees of freedom. Z is the statistical significance.

Solution	N^{sig}	δ	$2\Delta \log \mathcal{L}/N_f$	Z
I	838.5 ± 45.8	$-95.9^\circ \pm 1.5^\circ$	45.8/2	6.4σ
II	35.3 ± 9.3	$-152.1^\circ \pm 7.7^\circ$	45.8/2	6.4σ

any resonance, namely at 3.05, 3.06, 3.08, 3.083, 3.090 and 3.65 GeV. The other way is to use data from the $\psi(3770)$ resonance, assuming that the possible contribution $\psi(3770) \rightarrow \phi\pi^0$ is negligible. The selection criteria are the same except for the required 4-momenta in the kinematic fit. Neither sample shows significant $\phi\pi^0$ events. With a simultaneous fit, we obtain the QED contribution to the signal yield $N_{\phi\pi^0}^{\text{con}}(3.097) < 5.8$ at the 90% C.L., normalized according to the luminosity and efficiency and assuming the cross section is proportional to $1/s$ with s being the square of the c.m. energy. Thus we neglect the non-resonant QED contribution and use the upper limit of $N_{\phi\pi^0}^{\text{con}}(3.097)$ to estimate a systematic uncertainty from this assumption.

With the detection efficiency, $(45.1 \pm 0.2)\%$, obtained from the MC simulation, the branching fractions of $J/\psi \rightarrow \phi\pi^0$ are calculated to be $(2.94 \pm 0.16) \times 10^{-6}$ for Solution I and $(1.24 \pm 0.33) \times 10^{-7}$ for Solution II, where the errors are statistical only.

The sources of systematic uncertainty and their corresponding contributions to the measurement of the branching fraction are summarized in Table III. The tracking efficiency of charged kaons is studied using a high-purity control sample $J/\psi \rightarrow K_S^0 K^\pm \pi^\mp$, while the photon detection efficiency is investigated based on a clean sample of $J/\psi \rightarrow \rho\pi$. The differences between data and MC simulation are 1% for each charged track and 1% for each photon. The π^0 selection efficiency is studied with the sample $J/\psi \rightarrow \rho\pi$, and MC simulation agrees with data within 0.6%. The particle identification efficiency is studied with the sample $J/\psi \rightarrow \phi\eta \rightarrow K^+ K^- \gamma\gamma$. The efficiency difference between data and MC is 0.5%. To estimate the uncertainty associated with the kinematic constraint, a control sample of $J/\psi \rightarrow \phi\eta \rightarrow K^+ K^- \gamma\gamma$ is selected without a kinematic fit. The efficiency is the ratio of the signal yields with and without the kinematic requirement $\chi^2(4C) < 30$. The difference between data and MC, 3.2%, is assigned as the systematic uncertainty. For the uncertainties from the fit, alternative

fits are performed by varying the bin size and fit ranges. In addition, we also consider the effect from the parameterization of the function (F_{H_0}) for the null hypothesis, the relative phase angle δ and the decay width $\Gamma(m)$. We repeat fits parameterizing F_{H_0} with a third-order polynomial and extending δ in Eq. 1 to be $\delta + \delta_1 \frac{m-m_0}{\Gamma_0} + \delta_2 (\frac{m-m_0}{\Gamma_0})^2$ with two more parameters δ_1 and δ_2 . Assuming the modes $\phi \rightarrow K^+ K^- / K_S K_L$ have the same branching fraction 50%, we also perform a fit replacing $\Gamma(m)$ with $\Gamma_{K^+}(m) \times 50\% + \Gamma_{K^0}(m) \times 50\%$, where $\Gamma_{K^+}/K^0(m)$ is Eq. 3 using the mass of K^+/K^0 . The yield difference with respect to the nominal fit is taken as the systematic uncertainty due to the parameterization. The mass resolution, $\sigma_m = 1.00 \pm 0.02 \text{ MeV}/c^2$, is determined from $J/\psi \rightarrow \phi\eta$. Varying σ_m within $\pm 0.02 \text{ MeV}/c^2$ in the fit, the signal yield difference compared to the nominal fit is less than 1%. The QED contribution is neglected and the uncertainty for $N_{\phi\pi^0}^{\text{con}}(3.097)$ is taken as 5.8 as stated above. It contributes a systematic uncertainty of 0.7% (16.4%) for Solution I (II), ignoring the possible interference between the QED process and J/ψ resonance decay. The mass and width of the ϕ meson have been fixed to their world averages [17]. Changing them with 1σ uncertainty, the signal yield difference is taken as the systematic uncertainty. The meson radius r is 3 GeV^{-1} in the nominal fit. We change it from 1 GeV^{-1} to 5 GeV^{-1} , and the largest signal yield difference is 2.3% (3.0%) for Solution I (II). In the fit, the π^0 peaking background $J/\psi \rightarrow \gamma\eta_c(1S) \rightarrow \gamma K^+ K^- \pi^0$ is neglected. These background events can be subtracted by a MC simulation normalized according to the relevant branching fractions [17] and the efficiency. The signal yield difference is 1.1% (3.8%) for Solution I (II). We also consider the uncertainties from the number of J/ψ events and the branching fraction of $\phi \rightarrow K^+ K^-$. The total systematic uncertainty in Table III is the quadratic sum of the individual ones, assuming they are independent.

In summary, based on 1.31 billion J/ψ events collected with the BESIII detector, we perform an analysis of the decay $J/\psi \rightarrow \phi\pi^0 \rightarrow K^+ K^- \gamma\gamma$ and find a structure around $1.02 \text{ GeV}/c^2$ in the $K^+ K^-$ invariant mass spectrum. It can be interpreted as interference of $J/\psi \rightarrow \phi\pi^0$ with other processes decaying to the same final state. The fit yields two possible solutions and thus two branching fractions, $[2.94 \pm 0.16(\text{stat.}) \pm 0.16(\text{syst.})] \times 10^{-6}$ and $[1.24 \pm 0.33(\text{stat.}) \pm 0.30(\text{syst.})] \times 10^{-7}$.

Ref. [2] provides a model-independent relation, $\tilde{\mathcal{B}}(\phi\pi^0)/\tilde{\mathcal{B}}(\omega\pi^0) = (r_E \tan \theta_V - 1/\sqrt{2})^2 / (\tan \theta_V / \sqrt{2} + r_E)^2$. Here $\tilde{\mathcal{B}}(VP) \equiv$

TABLE III. Summary of branching fraction systematic uncertainties (in %).

Source	Solution I	Solution II
MDC tracking	2.0	2.0
Photon detection	2.0	2.0
Particle identification	0.5	0.5
π^0 's selection	0.6	0.6
Kinematic fit	3.2	3.2
Bin size	1.0	6.5
Fit range	1.0	15.3
Mass resolution	0.1	0.4
Parameterization of F_{H_0}	0	1.9
Parameterization of δ	0.9	1.6
Parameterization of $\Gamma(m)$	0.1	0.0
QED continuum	0.7	16.4
The mass and width of ϕ	0.8	0.1
The meson radius r	2.3	3.0
π^0 peaking background	1.1	3.8
Number of J/ψ	0.8	0.8
Uncertainty of $\mathcal{B}(\phi \rightarrow K^+ K^-)$	1.0	1.0
Total	5.5	24.4

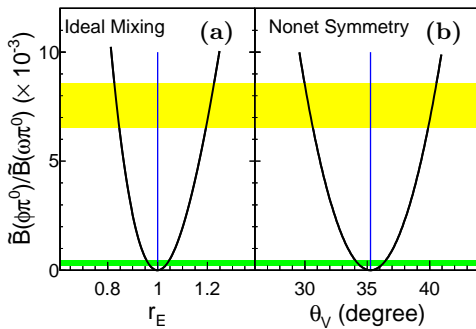


FIG. 3. Dependence of the reduced branching fraction ratio $\tilde{\mathcal{B}}(\phi\pi^0)/\tilde{\mathcal{B}}(\omega\pi^0)$ (a) on the nonet symmetry breaking strength r_E assuming $\omega - \phi$ ideal mixing and (b) on the mixing angle θ_V assuming nonet symmetry. The yellow (green) box represents Solution I (II). The blue line represents the nonet symmetry value in (a) and the ideal mixing angle in (b).

$\mathcal{B}(VP)/p_V^3$ is the reduced branching fraction of the decay $J/\psi \rightarrow VP$, and p_V is the momentum of the vector meson in the rest frame of J/ψ ; θ_V is the $\omega - \phi$ mixing angle; r_E is a dimensionless

parameter accounting for nonet symmetry breaking in the electromagnetic sector and $r_E = 1$ corresponds to nonet symmetry. We have used $\mathcal{B}(J/\psi \rightarrow \omega\pi^0) = (4.5 \pm 0.5) \times 10^{-4}$ [17]. If $\omega - \phi$ are mixed ideally, namely $\theta_V = \theta_V^{\text{ideal}} \equiv \arctan \frac{1}{\sqrt{2}}$, the nonet symmetry breaking strength is $\delta_E \equiv r_E - 1 = (+21.0 \pm 1.6)\%$ or $(-16.4 \pm 1.0)\%$ ($(+3.9 \pm 0.8)\%$ or $(-3.7 \pm 0.7)\%$) for Solution I (II), illustrated in Fig. 3 (a). On the other hand, we obtain $\phi_V \equiv |\theta_V - \theta_V^{\text{ideal}}| = 4.97^\circ \pm 0.33^\circ$ ($1.03^\circ \pm 0.19^\circ$) for Solution I (II) assuming nonet symmetry, shown in Fig. 3 (b). However, ϕ_V is found to be 3.84° from the quadratic mass formulae [17] and $3.34^\circ \pm 0.09^\circ$ from a global fit to the radiative transitions of light mesons [24]. The ϕ_V values do not agree with either solution. This is the first indication that nonet symmetry [2] is broken and the doubly OZI-suppression process contributes in J/ψ electromagnetic decays.

The BESIII collaboration thanks the staff of BEPCII and the IHEP computing center for their strong support. This work is supported in part by National Key Basic Research Program of China under Contract No. 2015CB856700; National Natural Science Foundation of China (NSFC) under Contracts Nos. 11125525, 11235011, 11322544, 11335008, 11425524; the Chinese Academy of Sciences (CAS) Large-Scale Scientific Facility Program; Joint Large-Scale Scientific Facility Funds of the NSFC and CAS under Contracts Nos. 11179007, U1232201, U1332201; CAS under Contracts Nos. KJCX2-YW-N29, KJCX2-YW-N45; 100 Talents Program of CAS; INPAC and Shanghai Key Laboratory for Particle Physics and Cosmology; German Research Foundation DFG under Contract No. Collaborative Research Center CRC-1044; Istituto Nazionale di Fisica Nucleare, Italy; Ministry of Development of Turkey under Contract No. DPT2006K-120470; Russian Foundation for Basic Research under Contract No. 14-07-91152; U. S. Department of Energy under Contracts Nos. DE-FG02-04ER41291, DE-FG02-05ER41374, DE-FG02-94ER40823, DESC0010118; U.S. National Science Foundation; University of Groningen (RuG) and the Helmholtzzentrum fuer Schwerionenforschung GmbH (GSI), Darmstadt; WCU Program of National Research Foundation of Korea under Contract No. R32-2008-000-10155-0

[1] S. Okubo, Phys. Lett. **5**, 165(1963); G. Zweig, CERN Report No. 8419/TH412 (1964); J. Iizuka, Prog. Theor. Phys. Suppl. **37**, 21 (1966).

[2] H. E. Haber, J. Perrier, Phys. Rev. D **32**, 2961 (1985).

[3] A. Seiden, Hartmut F.-W. Sadrozinski, H. E. Haber,

- Phys. Rev. D **38**, 824 (1988).
- [4] R. Escribano, Eur. Phys. J. C **65**, 467 (2010).
- [5] M. Ablikim *et al.* (BES Collaboration), Phys. Rev. Lett. **96**, 162002 (2006).
- [6] M. Ablikim *et al.* (BESIII Collaboration), Phys. Rev. D **87**, 032008 (2013).
- [7] D. Coffman *et al.* (MARKIII Collaboration), Phys. Rev. D **38**, 2695 (1988).
- [8] Q. Zhao, G. Li, C. H. Chang, Phys. Lett. B **645**, 173 (2007).
- [9] M. Ablikim *et al.* (BESIII Collaboration), Phys. Rev. D **71**, 032003 (2005).
- [10] M. Ablikim *et al.* (BESIII Collaboration), Chin. Phys. C **36**, 915 (2012).
- [11] The total number of J/ψ events taken in 2009 and 2012 is determined to be 1.311×10^9 with an uncertainty 0.8% with the same approach in Ref. [10].
- [12] M. Ablikim *et al.* (BESIII Collaboration), Nucl. Instrum. Meth. A **614**, 345 (2010).
- [13] G. Barrand *et al.*, Comput. Phys. Commun. **140**, 45 (2001).
- [14] S. Agostinelli *et al.* (GEANT4 Collaboration), Nucl. Instrum. Meth. A **506**, 250 (2003).
- [15] D. J. Lange, Nucl. Instrum. Meth. A **462**, 152 (2001).
- [16] R. G. Ping, Chin. Phys. C **32**, 599 (2008).
- [17] K. A. Olive *et al.* (Particle Data Group), Chin. Phys. C **38**, 090001 (2014).
- [18] J. C. Chen, G. S. Huang, X. R. Qi, D. H. Zhang, Y. S. Zhu, Phys. Rev. D **62**, 034003(2000).
- [19] $\frac{d^3\sigma}{d\cos\theta_\phi d\cos\theta_1 d\phi_1} = \sin^2\theta_1 [1 + \cos^2\theta_\phi + \sin^2\theta_\phi \cos(2\phi_1)]$, where θ_ϕ is the angle between the ϕ meson and the positron direction. θ_1 and ϕ_1 are the polar and azimuthal angles of the momentum of K with respect to the helicity direction of the ϕ meson.
- [20] F. James *et al.*, Statistic Methods in Experimental Physics (2^{nd} edition, World Scientific, 2007).
- [21] G. Cowan, Statistic Data Analysis (Clarendon Press, Oxford, 1998).
- [22] J. Blatt and V. Weisskopf, Theoretical Nuclear Physics (Wiley, New York, 1952).
- [23] S. S. Wilks, Annals of Math. Stat. **9**, 60 (1938).
- [24] F. Ambrosino *et al.*, (KLOE collaboration), J. High Energy Phys. **07**, 105 (2009).